



Gate electrostatics and quantum capacitance in ballistic graphene device

Caridad, Jose; Power, Stephen R.; Shylau, Artsem; Gammelgaard, Lene; Jauho, Antti-Pekka; Bøggild, Peter

Published in:
Physical Review B (Condensed Matter and Materials Physics)

Link to article, DOI:
[10.1103/PhysRevB.99.195408](https://doi.org/10.1103/PhysRevB.99.195408)

Publication date:
2019

Document Version
Peer reviewed version

[Link back to DTU Orbit](#)

Citation (APA):
Caridad, J., Power, S. R., Shylau, A., Gammelgaard, L., Jauho, A-P., & Bøggild, P. (2019). Gate electrostatics and quantum capacitance in ballistic graphene device. *Physical Review B (Condensed Matter and Materials Physics)*, 99(19), [195408]. <https://doi.org/10.1103/PhysRevB.99.195408>

General rights

Copyright and moral rights for the publications made accessible in the public portal are retained by the authors and/or other copyright owners and it is a condition of accessing publications that users recognise and abide by the legal requirements associated with these rights.

- Users may download and print one copy of any publication from the public portal for the purpose of private study or research.
- You may not further distribute the material or use it for any profit-making activity or commercial gain
- You may freely distribute the URL identifying the publication in the public portal

If you believe that this document breaches copyright please contact us providing details, and we will remove access to the work immediately and investigate your claim.

Gate electrostatics and quantum capacitance in ballistic graphene devices

José M. Caridad^{1†}, Stephen R. Power^{2,3,4}, Artsem A. Shylau¹, Lene Gammelgaard¹, Antti-Pekka Jauho¹, Peter Bøggild¹

¹*Center for Nanostructured Graphene (CNG), Department of Physics, Technical University of Denmark, 2800 Kongens Lyngby, Denmark*

²*Catalan Institute of Nanoscience and Nanotechnology (ICN2), CSIC and The Barcelona Institute of Science and Technology, Campus UAB, Bellaterra, 08193 Barcelona, Spain*

³*Universitat Autònoma de Barcelona, 08193 Bellaterra (Cerdanyola del Vallès), Spain*

⁴*School of Physics, Trinity College Dublin, Dublin 2, Ireland*

†corresponding author: jcar@dtu.dk

ABSTRACT. We experimentally investigate the charge induction mechanism across gated, narrow, ballistic graphene devices with different degrees of edge disorder. By using magnetoconductance measurements as the probing technique, we demonstrate that devices with large edge disorder exhibit a nearly homogeneous capacitance profile across the device channel, close to the case of an infinitely large graphene sheet. In contrast, devices with lower edge disorder (< 1 nm roughness) are strongly influenced by the fringing electrostatic field at graphene boundaries, in quantitative agreement with theoretical calculations for pristine systems. Specifically, devices with low edge disorder present a large effective capacitance variation across the device channel with a nontrivial, inhomogeneous profile due not only to

classical electrostatics but also to quantum mechanical effects. We show that such quantum capacitance contribution, occurring due to the low density of states (DOS) across the device in the presence of an external magnetic field, is considerably altered as a result of the gate electrostatics in the ballistic graphene device. Our conclusions can be extended to any two-dimensional (2D) electronic system confined by a hard-wall potential and are important for understanding the electronic structure and device applications of conducting 2D materials.

1. Introduction

An accurate picture of the electrostatic charge induction mechanism in field effect devices made of graphene or other two-dimensional (2D) crystals [1,2] is necessary to understand the physical properties of these novel nanomaterials [1-18] as well as to guide their exploitation in novel electronic [18], spintronic [19] and optoelectronic [20] applications. Yet, the precise details of the gate electrostatics are far from being understood in these atomically thin and finite-size systems [4-10]. In general, the relation between the gate voltage V_g and the induced average carrier density n is complicated in 2D materials, arising not only from classical electrostatic interactions but also from quantum mechanical effects related to modifications in their band structure under gating [7-10]. The relation $V_g(n)$ is a function of the total capacitance per area of the system C_{tot} and the elementary charge e and can be expressed in terms of classical (electrostatic) C_c and quantum capacitance C_q contributions as [8,9]:

$$V_g = en(C_c^{-1} + C_q^{-1}(n)) = enC_{tot}^{-1}(n) \quad (\text{Eq.1}),$$

where the dependence of C_q on n makes the capacitance-voltage relationship nonlinear in these systems [8,9]. Thus, C_{tot} is a carrier density dependent property, sensitive to the device geometry, edge morphology and external measurement conditions such as the presence of a magnetic field [9,10]. Furthermore, it exhibits local variations since the charge carrier density $n(\vec{r})$ is not uniform in these finite-size systems: $C_{tot}(\vec{r})/e \equiv \alpha_{tot}(\vec{r}) = n(\vec{r}) \cdot V_g^{-1}$ [5-8]. Here, \vec{r} represents the coordinate(s) in which the carrier density varies and α_{tot} represents the so-called lever arm of the system.

We focus on the capacitance-voltage characteristics of high-quality, ballistic devices made of graphene, the frontrunner of the 2D materials [1,2]. While the injection of charge carriers in graphene field effect devices is often approximated by the infinite parallel-plate capacitor model [1,2] where $n^\infty = \alpha_c^\infty V_g = (C_{ox}/e)V_g$ and C_{ox} is the gate oxide capacitance per unit area, the presence of hard-wall boundaries leads to accumulation of charges close to the device edges as a consequence of the fringing electrostatic field [7,8] (Fig. 1a). This results first in a generic, inhomogeneous and position dependent effective capacitance profile of classical origin $\alpha_c(x) = C_c(x)/e$ across the device channel (x direction) which qualitatively follows a divergent $1/\sqrt{x}$ dependence towards edges. Quantitatively, $\alpha_c(x)$ will depend on the entire device geometry, with the dominating factor being the ratio W/b between sample width W and the distance to the gate electrode b : $\alpha_c(x)$ increases for smaller W/b , especially for $W/b \leq 1$ [4, 7-9]. Second, the presence of this varying $\alpha_c(x)$ results in a nontrivial potential profile $U(x)$ across these devices, a fact that may lead to the presence (or even dominance) of a quantum contribution $\alpha_q(x) = C_q(x)/e$ within the total effective capacitance $\alpha_{tot}(x) = C_{tot}(x)/e$ of the system. [7-10]

Such complex gating dependencies are, however, largely unexplored and remain experimentally inconclusive. In particular, the existence of inhomogeneous capacitance profiles of classical origin $\alpha_c(x) = C_c(x)/e$ has been experimentally verified in high-quality, narrow graphene strips up to a certain modulation $\alpha_{tot}(x)^{(\max)} / \alpha_c^\infty = C_{tot}(x)^{(\max)} / C_{ox}$ [5], where $\alpha_{tot}(x)^{(\max)}$ is the maximum measured effective capacitance across the device. However, there are strong discrepancies between different experimental studies [3-6,11-17], and their correspondence with theoretical calculations, too [7-10]. Some studies exhibit capacitance profiles with modulation values across the device $\alpha_{tot}(x)^{(\max)} / \alpha_c^\infty \sim 2$, close to those given by classical electrostatic predictions [5]; others report much smaller capacitance modulations ($\alpha_{tot}(x)^{(\max)} / \alpha_c^\infty < 1.2$) across similar nanostructures [6], yet others observe no modulation at all ($\alpha(x) = \alpha_c^\infty$) [3], or simply neglect the effect by assuming a constant effective capacitance [11-13]. In a wider perspective, transport studies carried out in high-quality graphene devices display variations in how inhomogeneous gating is accounted for, whether these effects are included [4-6,14,15] or not at all [3,11-13,16,17] during the interpretation of the electrical measurements.

Here, we probe the total effective capacitance profile $\alpha_{tot}(x)$ across ballistic graphene nanoconstrictions (Fig.1b) with different degrees of edge disorder in a perpendicular magnetic field via magnetoconductance measurements. It is noteworthy that the local capacitance is accessible with these measurements in graphene devices [5, 6, 21], similar to conventional semiconductor structures defined in 2D electron gasses [5, 22]. Indeed, magnetoconductance measurements are particularly relevant for the characterization of narrow (≤ 150 nm) confined channels [22], where alternative magnetocapacitance techniques are limited due to several reasons. For instance, apart from possessing spatial resolution comparable or larger than the device size, scanning gate microscopy [23], single-electron transistor [24] or microwave impedance spectroscopy [14, 25]

measurements might affect or be affected by the actual device electrostatics. Specifically, by analyzing quantum Hall (QH) transport measurements [5,6] we show that devices with stronger edge disorder exhibit a nearly homogeneous effective capacitance profile, with $\alpha_{tot}(x)$ similar to α_c^∞ . In striking contrast and in quantitative agreement with theoretical predictions for disorder-free systems, devices with a lower degree of edge disorder (< 1 nm roughness) show an inhomogeneous effective capacitance consisting of both classical $\alpha_c(x)$ and quantum $\alpha_q(x)$ contributions. The presence of quantum capacitance effects in graphene devices is a direct consequence of the low density of states (DOS) of the system in a perpendicular magnetic field [10]. Also, $\alpha_q(x)$ is additionally influenced by band-structure modifications occurring in disorder-free, gated graphene devices; systems dominated by the electrostatic screening of the gate potential [4,10]. As shown below, the large $\alpha_c(x)$ diverging toward the edge is comparable in magnitude or larger than $\alpha_q(x)$ at low carrier densities and certain positions x across the channel of these clean devices, so that $\alpha_q(x)$ dominates the total effective capacitance (Eq.1).

2. Sample fabrication and magnetotransport measurements

We have fabricated graphene nanoconstrictions (Fig. 1b) with similar lengths L and widths W , $L=W \sim 100$ nm on hydrophobized SiO_2 substrates with thicknesses $b=100$ nm and with different degrees of edge disorder [4]. Our initial graphene is exfoliated on hydrophobic SiO_2 , resulting in flakes with mobilities ~ 20000 cm^2/Vs [4,26] and mean free paths l larger than L, W at $T = 4$ K ($l \sim 200$ nm [4,27]). Therefore, the transport of carriers through these devices is limited by boundary scattering [4]. Furthermore, we note that the edge roughness in these samples can be precisely

assessed via transmission electron microscopy [4], favoring their use in the present work with respect to nanoconstrictions [3] made from encapsulated graphene [28-30].

In particular, we study two types of nanoconstrictions, referred to as type S_{low} and type S_{high} made in an identical way except for the final etching step [4,31]. Sample type S_{low} was etched using reactive ion etching (40 sccm argon, 5 sccm oxygen), a procedure producing significantly less edge disorder than oxygen plasma ashing [4,31] technique used in sample type S_{high} . Further fabrication details of these devices can be found in [27] and in [4], where similar systems were studied. Measurements of differential magnetoconductance were performed at different magnetic fields using a Stanford SR830 lock-in amplifier with an excitation voltage of 100 μV at a frequency of 17.77 Hz in a cryostat at $T = 300\text{K}$ and $T = 4\text{ K}$.

Figs. 1c,d show the magnetoconductance G as a function of V_g for the two sample types at different perpendicular magnetic fields B . The effect of edge disorder reflects itself in the magnitude of the conductance $G(V_g)$, which is more than two times smaller in type S_{high} (Fig. 1c) compared to type S_{low} (Fig. 1d) at any B and V_g . Furthermore, sample type S_{high} shows a quantized conductance $G = G(V_g)$ at high B for the zeroth-order Landau level, $LL0$, at the corresponding filling factor for graphene: $\nu = 2$. This plateau is followed by a conductance dip due to the presence of a nonzero longitudinal conductivity in the two-terminal device, effect that depends on the device geometry [4, 32]. For the higher LLs , G is smaller than the expected quantized value due to the pronounced effect of edge disorder [4], promoting backscattering between edge channels [33]. In contrast, as reported in our previous study [4], sample type S_{low} (edge roughness $< 1\text{ nm}$) shows a conductance the value of which is larger than the value expected for the single-electron picture and does not exhibit quantization. This effect, referred to as conductance quantization suppression

(CQS) [4,34], is a manifestation of additional, overlapping and counter-propagating conducting channels in the constriction. These channels emerge from a qualitative modification of the bandstructure of the system in the quantum Hall regime due to fringe field effects occurring in ballistic systems with low edge disorder [4,34] (see [27]). As such, their appearance is symptomatic of and relies on the presence of a large and inhomogeneous capacitance profile across the nanoconstrictions [4,34].

3. Effective capacitance profile

We experimentally probe $\alpha_{tot}(x)$ in both types of samples S_{low} and S_{high} by using the evolution of the magnetotransport data shown in Figs.1c,d with respect to different B (the selected positions of $G(V_g, B)$ are marked by arrows). This is possible thanks to the extreme sensitivity of the QH transport to the carrier density and carrier density distributions [5,6]. Briefly [5,6], in the QH regime, when the Fermi level lies in-between two LLs and the conduction is governed by ν propagating edge states, each edge channel probes a different spatial region from the edge of the device [5], whereas the bulk is insulating [5,6]. On the one hand, the carrier density n_ν for a filling factor ν is given by $n_\nu = \nu e B h^{-1}$ with a corresponding effective capacitance $\alpha_\nu = n_\nu (V_g - V_{CNP})^{-1}$, where V_{CNP} is the charge neutrality point of the device. On the other hand, an estimate of the position of these edge-channels is given by corresponding cyclotron diameter $d_\nu = (\nu h)^{1/2} (e \pi B)^{-1/2}$ for graphene [5,6]. As the capacitance increase is linked to the charge accumulation across the channel of finite-size graphene devices, edge states of different LLs probe different spatial regions of the device and are subjected to a different effective capacitance. Thus, by making the assignment $\alpha_\nu \equiv \alpha(x = d_\nu)$, the profile of $\alpha_{tot}(x)$ across the device can be

experimentally assessed [5,6]. Such capacitance mapping is clear in the absence of back-scattering characteristic of the QH regime.

We argue that this semi-classical method can be also used in our ballistic devices exhibiting the CQS effect (Sample type S_{low} , Fig. 1d). This is particularly valid at gate voltages where the (nonquantized) conductance shows a maximum (arrows in Fig. 1d) $G^{(\text{max})}$, places where, if existent, backscattering between the counter propagating edge channels in the system is weakest [4,34] (see [27]). As such, the link between G and $n(x)$ is still valid by taking $\nu(x) \sim G^{(\text{max})}(e^2/h)$, and the capacitance profile $\alpha_{\text{tot}}(x)$ can then be extracted as demonstrated below when comparing the experimental values with the corresponding theoretical calculations.

Fig. 2 shows the extracted effective capacitance α_v versus d_v plotted for the different LLs in our samples with high and low edge disorder. Samples with high edge disorder (sample type S_{high} , Fig. 2a) show a slowly monotonically increasing capacitance $\alpha_v(d_v)$ towards edges, with quantitative values close to those of the infinite parallel-plate capacitor, α_c^∞ (green dotted line). Specifically, this capacitance profile is nearly homogeneous across the device channel (x direction), with only a small measured modulation up to $\alpha_{\text{tot}}(x)^{(\text{max})} / \alpha_c^\infty \sim 1.2$ for $LL0$. In contrast, devices with low edge disorder (sample type S_{low} , Fig.2b) exhibit an inhomogeneous capacitance profile, with much larger modulations ($\alpha_{\text{tot}}(x)^{(\text{max})} / \alpha_c^\infty \sim 2.5$ for the case of $LL0$ and ~ 1.7 for $LL1$). Moreover, we note how the capacitance profile is nonmonotonic in these samples for $LL0$.

Three initial conclusions can be drawn from the experimental data shown in Fig.2, all of them consistent with a more pronounced capacitance profile for sample type S_{low} as compared to S_{high} .

(i) As expected from an electrostatic point of view [6,35], there exists electron-hole ($e^- - h^+$)

symmetry in both type of samples. The difference in capacitances observed for e^- and h^+ is lower than 10% with respect to the absolute capacitance at any B (ii) The lowest LL ($LL0$) is closest to the edge, where more charge is expected to accumulate [4-8]. Consequently, for a constant B , α_v exhibits a higher absolute value for $LL0$ than for $LL1$ in sample type S_{low} . In addition, (iii) for a varying B , the capacitance variation of $LL0$ is the largest as well.

Next, we analyze in more detail the capacitance profile $\alpha_v(d_v)$ in both types of devices. For $LL0$, the small modulation $\alpha_{\text{tot}}(x)^{(\text{max})} / \alpha_c^\infty \sim 1.2$ in devices of sample type S_{high} differs quantitatively from the electrostatic capacitance $\alpha_c(x)$ calculated for our constriction geometry, which is monotonic and diverges rapidly towards edges (Fig. 3, blue line; simulation details in [27]). Such behavior is attributed to scattering from edge defects, decreasing the charge accumulation in a similar manner as seen for low quality devices with disorder in the channel [5,6]. This result explains the fact that some high-quality devices in literature exhibit effective capacitances resembling the one from an infinite parallel-plate capacitor α_c^∞ [3,4].

Then, we note that despite having a large modulation, the capacitance variation in sample type S_{low} does not completely follow the trend of the calculated classical electrostatic capacitance $\alpha_c(x)$ either: rather than following a divergent $1/\sqrt{x}$ dependence towards the edge [7,8] the measured capacitance α_v has a nonmonotonic profile, decreasing more rapidly than $\alpha_c(x)$ for distances close to the edge and in the middle of the channel. Moreover, α_v exhibits some values smaller than α_c^∞ at the central part of the constriction (distances > 35 nm from the edge) for $LL0$ but not for $LL1$. In addition, α_v shows a maximum $\alpha_v^{(\text{max})}$ at a position $d_{v,\text{max}} \sim 24$ nm from the edge, with α_v smaller than $\alpha_v^{(\text{max})}$ for $d_v < d_{v,\text{max}}$. We do not expect this extremal value to be caused by the breakdown of

the classical capacitance $\alpha_c(x)$ at distances from edges given by the magnetic length $l_B = \hbar^{1/2}(eB)^{-1/2}$ [7]: $d_{v,\max}$ is three times larger than l_B at the corresponding B (10 T) at which the maximum is observed. This argument is additionally supported by the fact that no local maximum is experimentally observed in sample type S_{high} (Fig.2a) despite the minimum measured d_v in such samples (15 nm) being smaller than $d_{v,\max}$.

4. Effective capacitance calculation: classical and quantum capacitance contributions

We demonstrate that the mismatch between the calculated electrostatic capacitance (Fig. 3, blue line) and the experimentally probed capacitance of sample type S_{low} at the *LL0* (Fig 2b, black circular dots and Fig 3, inset) can be fully accounted for by including quantum contributions to the total capacitance of the system. Such quantum contributions, arising due to the low local DOS [36-39] across the quasi- one dimensional system [10], are not only dependent on the presence of external magnetic fields B but also heavily affected by the electrostatic screening of the gate potential [4,34] (see [27]).

We calculate the quantum capacitance contribution [27] $\alpha_q(x)$ across the ballistic, gated devices at $B = 10\text{T}$ and low carrier densities (*LL0*) (Fig. 3, red line). First, we show that both classical and quantum contributions are comparable in magnitude and coincide at two distances: ~ 25 nm far from the edge and at the central part of the nanodevice (~ 40 nm far from the edge). By using Eq.1, we calculate the total effective capacitance $\alpha_{\text{tot}}(x)$ of these devices (Fig. 3, black curve), which is in quantitative agreement (below $\sim 30\%$ mismatch) with our experimental data $\alpha_v(d_v)$ for *LL0* (Fig 2b and Fig. 3, inset). Specifically, $\alpha_{\text{tot}}(x)$ shows a clear maximum $\alpha_{\text{tot}}^{(\max)}(x_1)$ at a position $x_1 \sim 25$ nm, close to $d_{v,\max}$. For closer distances ($x < x_1$) towards the edge at $x = 0$, $\alpha_{\text{tot}}(x)$ is dominated by

quantum contributions since $\alpha_c(x) > \alpha_q(x)$. Instead, for distances $x_1 < x < x_2$ with $x_2 \sim 32$ nm, $\alpha_{tot}(x)$ is mostly dominated by the classical capacitance profile, since $\alpha_c(x) < \alpha_q(x)$ in this interval. Furthermore, for distances $x > x_2$ (central part of the nanoconstriction) $\alpha_{tot}(x)$ is again dominated by the quantum contribution due to the vanishing local DOS at these positions. This argument explains the fact that experimentally, α_v for *LL0* is smaller than α_c^∞ at the central part of the constriction, too. Finally, for completeness, we note that the experimental capacitance profile α_v shown for *LL1* in samples S_{low} (Fig 2b, red triangles) increases monotonically towards edges, similar to the classical profile. This behavior is due to the fact that the quantum contribution to the capacitance for *LL1* is larger than the classical one [27] for the probed distances from the edge $x \equiv d_v$ (between 30 and 40 nm). Thus, the classical contribution dominates the total effective capacitance profile at these higher carrier densities (*LL1*).

5. Conclusions

In summary, by analyzing quantum Hall transport measurements, we have extracted the total effective capacitance profile across ballistic graphene devices. Such profiles heavily depend on the edge disorder level in the device. In particular, similar to diffusive devices, ballistic samples with a large edge roughness show a nearly homogeneous capacitance with small modulation and values close to the infinite parallel-plate capacitor. In contrast, in excellent agreement with calculations for pristine and gated systems, narrow ballistic devices with low edge disorder (< 1 nm roughness) show an effective capacitance profile with a much larger modulation due to an enhanced impact of the fringe field effects at graphene edges. This profile is nonmonotonic at low carrier densities due to the interplay between classical and quantum capacitance contributions across the gated device even when using relatively thick (100 nm) dielectric layers [8,9]. Despite being demonstrated in ballistic graphene nanoconstrictions, our conclusions can be extended to other systems with sharp

edge potential [4,7,8,34], and thus, our findings can help to understand the electronic properties of other types of gated nanostructures made from 2D materials [40,41] or other 2D systems [42].

Acknowledgements We acknowledge stimulating discussions with K. Kaasbjerg. This work was supported by the Danish National Research Foundation Center for Nanostructured Graphene, project DNRF103, and the Union's Horizon 2020 research and innovation programme (grant agreement No GrapheneCore2 785219). J.M.C. acknowledges funding from the Øtto Monsteds Fond. S.R.P. acknowledges funding from the European Union's Horizon 2020 research and innovation programme under the Marie Skłodowska-Curie grant agreement No 665919 and from the Irish Research Council under the laureate awards programme.

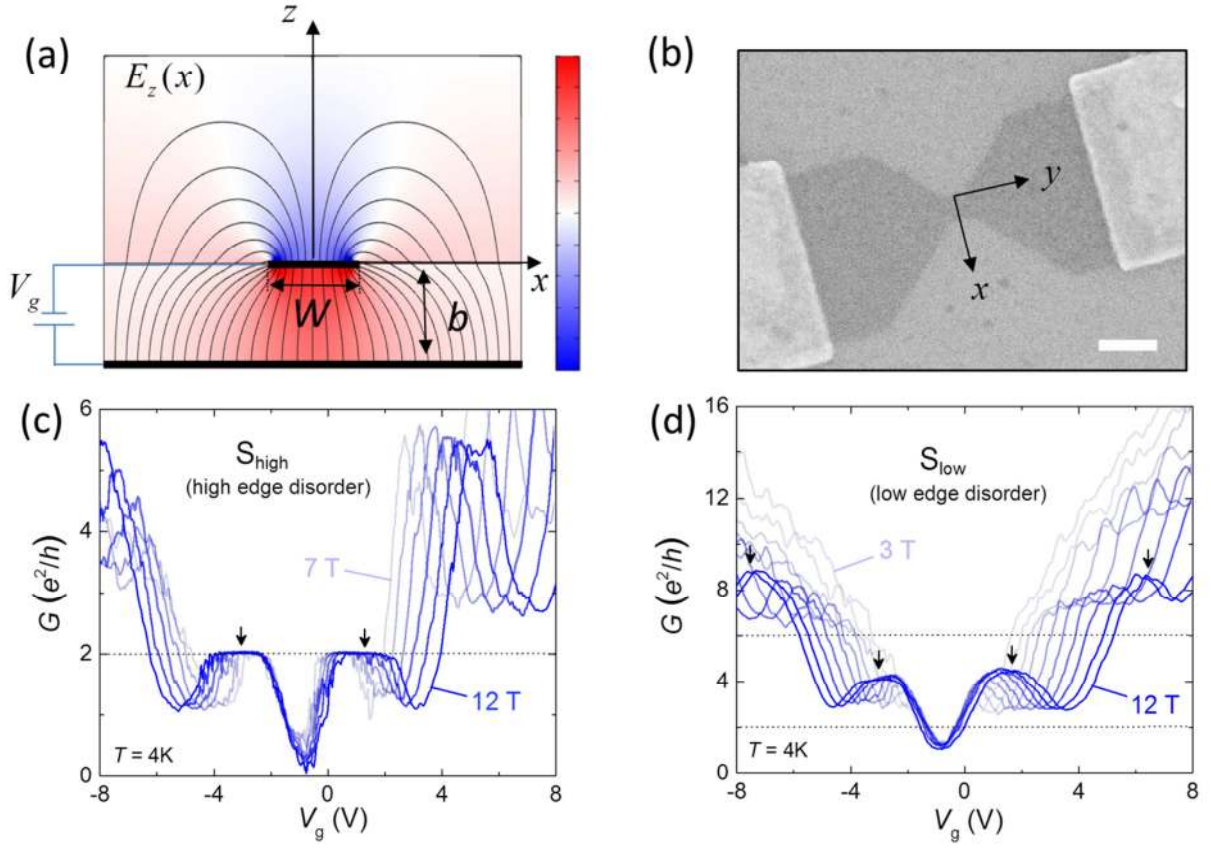


Fig. 1. Sample fabrication and electrical characterization (a) Electric field distribution $E_z(x)$ around a gated graphene device with $b=W=100$ obtained by solving the Poisson equation in the device [27]. (b) Scanning electron micrograph of a graphene nanoconstriction device. Scale bar is 200 nm. (c) Conductance G vs gate voltage V_g in a nanoconstriction of type S_{high} at different magnetic fields (from 7 to 12 T in steps of 1T) at $T = 4$ K. (d) Conductance G vs gate voltage V_g in a nanoconstriction of type S_{low} at different magnetic fields (from 3 to 12 T in steps of 1T) at $T = 4$ K. Arrows in panels (c) and (d) indicate the experimental points (V_g, G) taken to calculate $\alpha_\nu(d_\nu)$ in Fig. 2 for $B = 12$ T, i.e. center of the plateau for sample S_{high} [5,6] and G^{max} for S_{low} . Corresponding points are taken for other magnetic fields. Dotted lines indicate the expected quantization values for graphene.

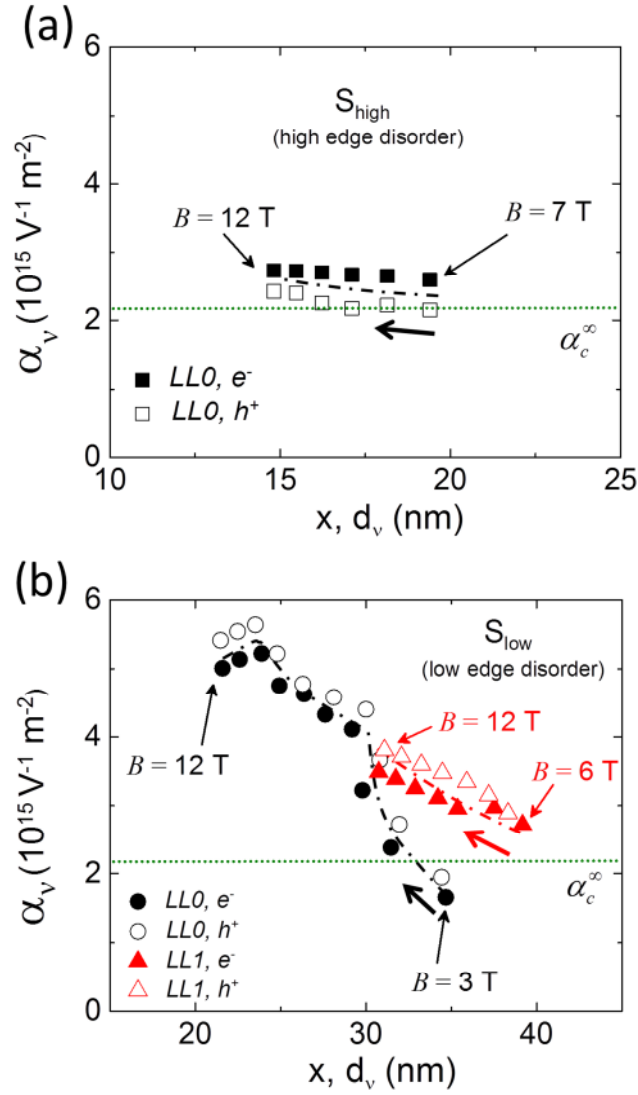


Fig. 2. Experimental effective capacitance α_v across the nanoconstrictions for different Landau levels (LL s) for electrons (e^-) and holes (h^+) at positions x corresponding to the cyclotron diameter d_v . (a) Sample type S_{high} . B varies from 7 to 12 T increasing in 1-T steps. $B = 7 \text{ T}$ is the minimum B to observe a conductance plateau for $LL0$ in samples S_{high} . (b) Sample type S_{low} . B varies from 3 to 12 T ($LL0$) and from $B = 6 \text{ T}$ to $B = 12 \text{ T}$ ($LL1$) in 1-T steps. $B = 3 \text{ T}$ and $B = 6 \text{ T}$ are the minimum fields to observe the CQS regime in these samples for $LL0$ and $LL1$,

respectively. Green dotted lines in both panels show the capacitance value for an infinite parallel-plate capacitor $\alpha_c^\infty = \frac{C_{ox}}{e} = 2.19 \times 10^{15} \text{ V}^{-1} \text{ m}^{-2}$. Dash-dotted lines represent a guide to the eye.

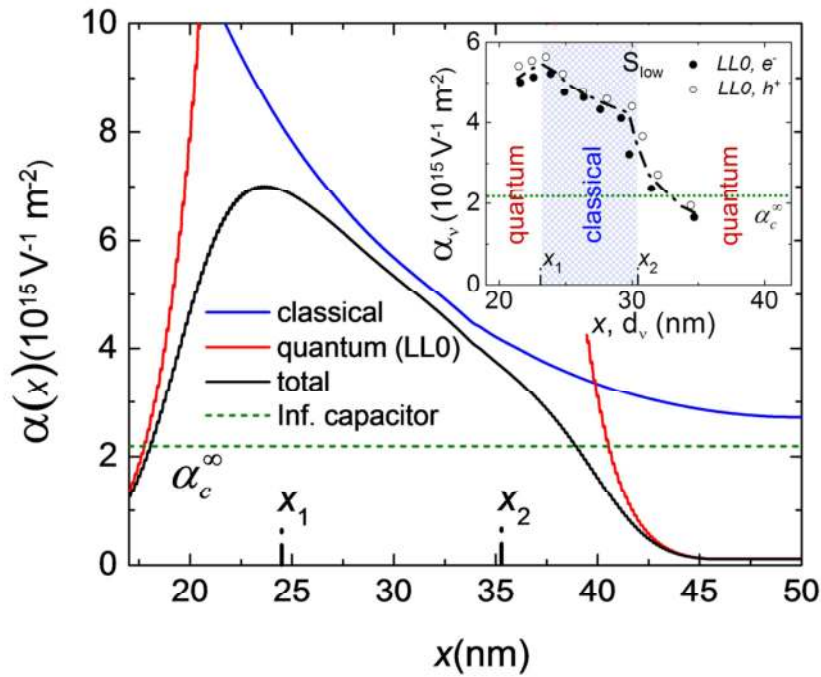


Fig. 3. Capacitance profile across the nanoconstrictions of type S_{low} for $LL0$. Calculated classical (blue curve), quantum (red curve) and total effective capacitance (black curve) profiles across a graphene nanoconstriction with $W = 100 \text{ nm}$. The constant dashed green line represents α_c^∞ . The inset shows the experimental data for sample type S_{low} (Fig. 2b), separating zones where classical (blue) or quantum (red) contributions dominate according to the prediction shown in the main figure. Dash-dotted lines represent a guide to the eye.

References

1. K. S. Novoselov, A. K. Geim, S. V. Morozov, D. Jiang, Y. Zhang, S. V. Dubonos, I. V. Grigorieva, and A. A. Firsov. Electric field effect in atomically thin carbon films. *Science* 306, 666 (2004)
2. Y. Zhang, Y. Tan, H. L. Stormer and P. Kim. Experimental observation of the quantum Hall effect and Berry's phase in graphene. *Nature* 438, 201 (2005).
3. B. Terrés, L.A. Chizhova, F. Libisch, J. Peiro, D. Jörger, S. Engels, A. Girschik, K. Watanabe, T. Taniguchi, S.V. Rotkin, J. Burdörfer and C. Stampfer. Size quantization of Dirac fermions in graphene constrictions. *Nature Comm.* 7, 11528 (2016).
4. J.M. Caridad, S.R. Power, M.R. Lotz, A.A. Shylau, J.D. Thomsen, L. Gammelgaard, T.J. Booth, A-P. Jauho and P. Bøggild. Conductance quantization suppression in the quantum Hall regime. *Nature. Comm.* 9, 659 (2018).
5. I.J. Vera-Marun, P.J. Zomer, A. Veligura, M.H.D. Guimarães, L. Visser, N. Tombros, H.J. van Elferen, U. Zeitler and B.J. van Wees. Quantum Hall transport as probe of capacitance profile at graphene edges. *Appl. Phys. Lett.* 102, 013106 (2013).
6. C. Barraud, T. Choi, P. Butti, I. Shorubalko, T. Taniguchi, K. Watanabe, T. Ihn and K. Ensslin. Field effect in the quantum Hall regime of a high mobility graphene wire. *J. Appl. Phys.* 116, 073705 (2014).
7. P.G. Silvestrov and K.B. Efetov. Charge accumulation at the boundaries of a graphene strip induced by a gate voltage: Electrostatic approach. *Phys. Rev. B*, 77, 155436 (2008).
8. J. Fernández-Rossier, J.J. Palacios and L. Brey. Electronic structure of gated graphene and graphene nanoribbons. *Phys. Rev. B* 75, 205441-205448 (2007).
9. A.A.Shylau, J.W. Klos and I.V. Zozoulenko. Capacitance of graphene nanoribbons. *Phys. Rev. B* 80, 205402 (2009)

10. J. Guo, Y. Yoon and Y. Ouyang. Gate Electrostatics and Quantum Capacitance of Graphene Nanoribbons. *NanoLett.* **7**, 1935 (2007).
11. K.I. Bolotin, K.J. Sikes, Z. Jiang, M. Klima, G. Fudenberg, J. Hone, P. Kim and H.L. Stormer. Ultrahigh electron mobility in suspended graphene. *Solid State Commun.* **146**, 351 (2008).
12. X. Du, I. Skachko, A. Barker and E.Y. Andrei. Approaching ballistic transport in suspended graphene. *Nat. Nanotechnol.* **3**, 491 (2008).
13. B.E. Feldman, J. Martin and A. Yacoby. Broken-symmetry states and divergent resistance in suspended bilayer graphene. *Nat. Phys.* **5**, 899 (2009).
14. Y-T. Cui, B. Wen, E.Y. Ma, G. Diankov, Z. Han, F. Amet, T. Taniguchi, K. Watanabe, D. Goldhaber-Gordon, C. R. Dean and Z-X. Shen. Unconventional correlation between quantum Hall transport and bulk state filling in gated graphene devices. *Phys. Rev. Lett.*, **117**, 18661 (2016).
15. T. Taychatanapat, K. Watanabe, T. Taniguchi and P. Jarillo-Herrero. Electrically tunable transverse magnetic focusing in graphene. *Nature Phys.*, **9**, 225 (2013).
16. H. Hettmansperger, F. Duerr, J.B. Oostinga, C. Gould, B. Trauzettel and L.W. Molenkamp. Quantum Hall effect in narrow graphene ribbons. *Phys. Rev. B.* **8**, 195417 (2012).
17. N. Tombros, A. Veligura, J. Junesh, M.H.D. Guimarães, I.J. Vera-Marun, H.T. Jonkman and B.J. van Wees. Quantized conductance of a suspended graphene nanoconstriction. *Nature Phys.* **7**, 697 (2011).
18. J.M. Caridad, G. Calogero, P. Pedrinazzi, J.E. Santos, A. Impellizzeri, T. Gunst, T.J. Booth, R. Sordan, P. Bøggild, M. Brandbyge. A graphene-edge ferroelectric molecular switch. *NanoLett.* **18**, 4675 (2018)

19. A. Dankert and S.P.Dash. Electrical gate control of spin current in van der Waals heterostructures at room temperature. *Nature Comm.* 8, 16093 (2017).
20. B. Yao, Y. Liu, S-W. Huang, C. Choi, Z. Xie, J.F. Flores, Y. Wu, M. u, D-L. Kwong, Y. Huang, Y. Rao, X. Duan and C.W. Wong. Broadband gate-tunable terahertz plasmons in graphene heterostructures. *Nature Phot.* 12, 22 (2018)
21. S. Ihnatsenka and I.V. Zozoulenko. Spin polarization and g-factor enhancement in graphene nanoribbons in a magnetic field. *Phys. Rev. B* 86, 155407 (2012)
22. K.F. Berggren, G. Roos and H. van Houten. Characterization of very narrow quasi-one-dimensional quantum channels. *Phys. Rev. B*, 37, 10118 (1998)
23. A.G.F. Garcia, M, Köning, D. Goldhaber-Gordon and K. Tood. Scanning gate microscopy of localized states in wide graphene constrictions. *Phys. Rev. B*, 87, 085446 (2013)
24. J.Martin, N. Akerman, G. Ulbrich, T. Lohmann, K. von Klitzing, J.H. Smet and A. Yacoby. *Nat. Physics* 5, 699 (2009)
25. E. Y. Ma, M. Reyes Calvo, J. Wang, B. Lian, M. Mühlbauer, C. Brüne, Y-T. Cui, K. Lai, W. Kundhikanjana, Y. Yang, M. Baenninger, M. König, C. Ames, H. Buhmann, P. Leubner, L.W. Molenkamp, S-C. Zhang, D. Goldhaber-Gordon, M.A.Kelly and Z-X. Shen. Unexpected edge conduction in mercury telluride quantum wells under broken time-reversal symmetry. *Nature Comm.* 6, 7252 (2015).
26. J.M. Caridad, S. Connaughton, C. Ott, H.B. Weber and V. Krstić. An electrical analogy to Mie scattering. *Nature Comm.* 7, 12894-12900 (2016).
27. See Supplement Material at [URL will be inserted by publisher] for additional experimental data, discussion about the validity of the semi-classical method to probe capacitance profiles and calculation of classical and quantum capacitances.

28. L. Wang, I. Meric, P. Y. Huang, Q. Gao, Y. Gao, H. Tran, T. Taniguchi, K. Watanabe, L. M. Campos, D. A. Muller, J. Guo, P. Kim, J. Hone, K. L. Shepard, and C. R. Dean. One-dimensional electrical contact to a two-dimensional material. *Science* 342, 614 (2013)
29. F. Pizzocchero, L. Gammelgaard, B. S. Jessen, J. M. Caridad, L. Wang, J. Hone, P. Bøggild, and T. J. Booth. The hot-pick up technique for batch assembly of van der Waals heterostructures. *Nature Comm.* 7, 11894 (2016)
30. P. Pedrinazzi, J.M. Caridad, D.M.A. Mackenzie. F. Pizzocchero, L. Gammelgaard, B.S. Jessen, R. Sordan, T.J. Booth and P. Bøggild. High-quality graphene flakes exfoliated on a flat hydrophobic polymer. *Appl. Phys. Lett.* 3, 033101 (2018).
31. P. Simonet, D. Bischoff, A. Moser, T. Ihn and K. Ensslin. Graphene nanoribbons: relevance of etching process. *J.Appl. Phys.* **117**, 184303-184307 (2015).
32. J.R. Williams, D.A. Abanin, L. DiCarlo, L.S. Levito and C.M Marcus, C.M. Quantum Hall conductance of two-terminal graphene devices. *Phys. Rev. B* **80**, 045408 (2009)
33. H. Shen, A. Cresti, W. Escoffier, Y. Shi, X. Wang and B. Raquet. Peculiar magnetotransport features of ultranarrow graphene nanoribbons under high magnetic field. *ACS Nano*, **10**, 1853-1858 (2015).
34. A.A. Shylau, I.V.Zozoulenko, H.Xu and T. Heinzl. Generic suppression of conductance quantization of interacting electrons in graphene nanoribbons in a perpendicular magnetic field. *Phys. Rev. B* **82**, 121410 (2010)
35. S. Slizovskiy and V. Fal'ko. Suppressed compressibility of quantum Hall effect edge states in epitaxial graphene on SiC. *Phys. Rev. B* 97, 075404 (2018)
36. S. Dröscher, P. Roulleau, F. Molitor, P. Struderus, C. Stampfer, K. Ensslin and T. Ihn. Quantum capacitance and density of states of graphene. *Appl. Phys. Lett.* **96**, 152104 (2010)

37. R. Reiter, U. Derra, S. Birner, B. Terrés, F. Libisch, J. Burgdörfer and C. Stampfer. Negative quantum capacitance in graphene nanoribbons with lateral gates. *Phys. Rev. B* **84**, 115406 (2014)
38. J. Xia, F. Chen, J. Li and N. Tao. Measurement of the quantum capacitance of graphene. *Nat. Nanotechnol.* **4**, 505 (2009)
39. G.L. Yu, R. Jalil, B. Belle, A.S. Mayorov, P. Blake, F. Schedin, S.V. Morozov, L.A. Ponomarenko, F. Chiappini, S. Wiedmann, U. Zeitle, M.I. Katsnelson, A.K. Geim, K.S. Novoselov and D.C. Elias. Interaction phenomena in graphene seen through quantum capacitance. *Proced. Nat. Acad. Sci.* **110**, 3282 (2013)
40. K.S. Novoselov and A.H. Castro Neto. Two-dimensional crystal-based heterostructures: materials with tailored properties. *Phys. Scr.* 2012, 014006 (2012)
41. S. Rasappa, J.M. Caridad, L. Schulte, A. Cagliani, D. Borah, M.A. Morris, P. Bøggild and S. Ndoni. *RSC Advances*, **5**, 82, 66711 (2015)
42. T. Akiho, H. Irie, K. Onomitsu and K. Muraki. Counterflowing edge current and its equilibration in quantum Hall devices with sharp edge potential: roles of incompressible strips and contact configuration. *Phys. Rev. B*, **99**, 121303 (2019)

Supplementary Information

Gate electrostatics and quantum capacitance in ballistic graphene devices

José M. Caridad^{1†}, Stephen R. Power^{2,3,4}, Artsem A. Shylau¹, Lene Gammelgaard¹, Antti-Pekka Jauho¹, Peter Bøggild¹

¹*Center for Nanostructured Graphene (CNG), Department of Physics, Technical University of Denmark, 2800 Kongens Lyngby, Denmark*

²*Catalan Institute of Nanoscience and Nanotechnology (ICN2), CSIC and The Barcelona Institute of Science and Technology, Campus UAB, Bellaterra, 08193 Barcelona, Spain*

³*Universitat Autònoma de Barcelona, 08193 Bellaterra (Cerdanyola del Vallès), Spain*

⁴*School of Physics, Trinity College Dublin, Dublin 2, Ireland*

†corresponding author: jcar@dtu.dk

1. Experimental details

Fabrication and electrical characteristics of devices prior to define nanoconstrictions

Devices with field-effect mobility $\mu \sim 20.000 \text{ cm}^2/\text{Vs}$ (estimated mean free paths $l \sim 200 \text{ nm}$) at a temperature $T = 4\text{K}$ are achieved by the mechanical exfoliation of graphene on hydrophobic Si/SiO₂ substrates. [S1,S2] We select devices with relatively low contact resistances R_c below 600Ω . These initial device parameters (μ , R_c) are extracted [S2] by first shaping, contacting and measuring the transport properties of rectangular two-terminal

devices with a width W of $\sim 1 \mu\text{m}$ (Fig. S1a), where the obtained two point resistance R_{2pt} is fitted to the equation [S3]:

$$R_{2pt} = R_c + \frac{L/W}{e\mu\sqrt{n^2 + n_{res}^2}} \quad (\text{Eq.S1}).$$

Here, e is the elementary charge, n_{res} is the residual carrier concentration and n is the back-gate induced carrier concentration given by:

$$n = \frac{C_{ox}}{e} (V_g - V_{CNP}) \quad (\text{Eq. S2}),$$

where C_{ox} is the gate oxide capacitance per unit area for an infinite parallel-plate capacitor ($3.5 \times 10^{-4} \text{ Fm}^{-2}$ for our 100nm thick SiO_2) and V_{CNP} is the position of the charge neutrality point (CNP). Fig S1b shows the two-point conductance of the device, given by $G = 1/[R_{2pt} - R_c]$, at two different temperatures: 4K and 300 K. The decreased conductance exhibited at higher temperatures is ascribed to a decrease in the intrinsic mobility of these samples due to the role of electron-phonon scattering [S2].

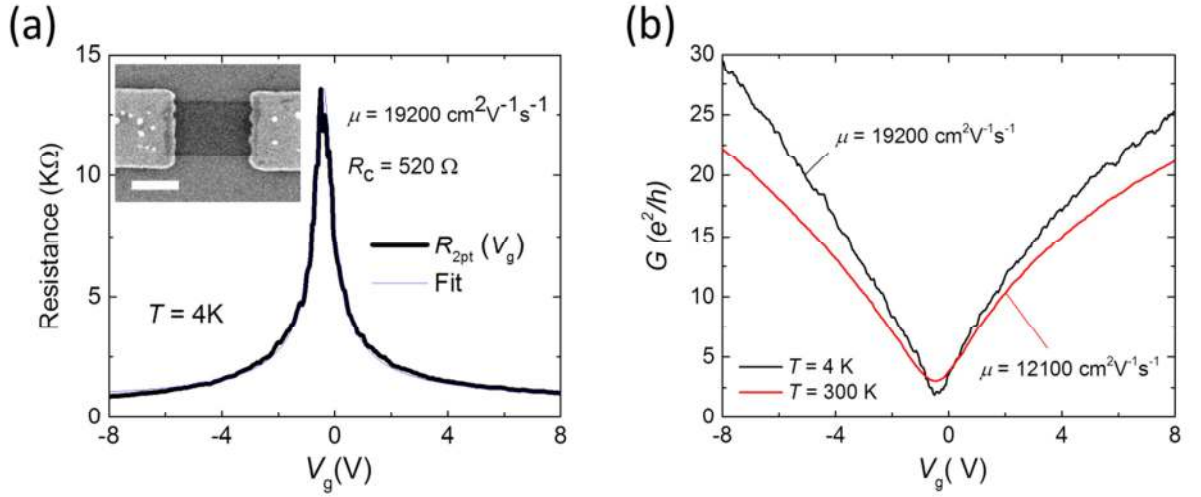


Fig.S1. (a) Two-point (2-pt) resistance of pre-constriction devices (graphene strips with width $W = 1 \mu\text{m}$) at $T = 4 \text{ K}$ and $B = 0 \text{ T}$. Fitting the experimental data with Eq. S1, we extract a $\mu = 19200 \text{ cm}^2/\text{Vs}$ and a $R_c = 520 \Omega$. Inset shows a scanning electron micrograph of this device. Contacts made from Ti/Au (5/25 nm). Scale bar is $1 \mu\text{m}$. (b) Conductance of these devices at two temperatures ($T = 4\text{K}$ and $T = 300\text{K}$) and $B = 0 \text{ T}$.

Furthermore, we measure the magnetoconductance $G(V_g, B)$ of these wide graphene devices for different magnetic fields (Fig. S2a). First, this is done as an alternative method to extract the value of contact resistance in the device R_c . Then, from this data (Fig. 2a), we can also extract the effective capacitance of these large (and diffusive) devices following the procedure described in the main text. Fig.2b shows how this effective capacitance is nearly homogeneous, close to the values of the infinite parallel-plate capacitor and exhibits a small measured modulation below $\alpha_{tot}(x)^{(\text{max})} / \alpha_c^\infty < 1.2$ for both $LL0$ and $LL1$. These trends are expected from an electrostatic point of view for samples with $W/b \gg 1$ and are consistent with similar samples reported in literature [S4, S5].

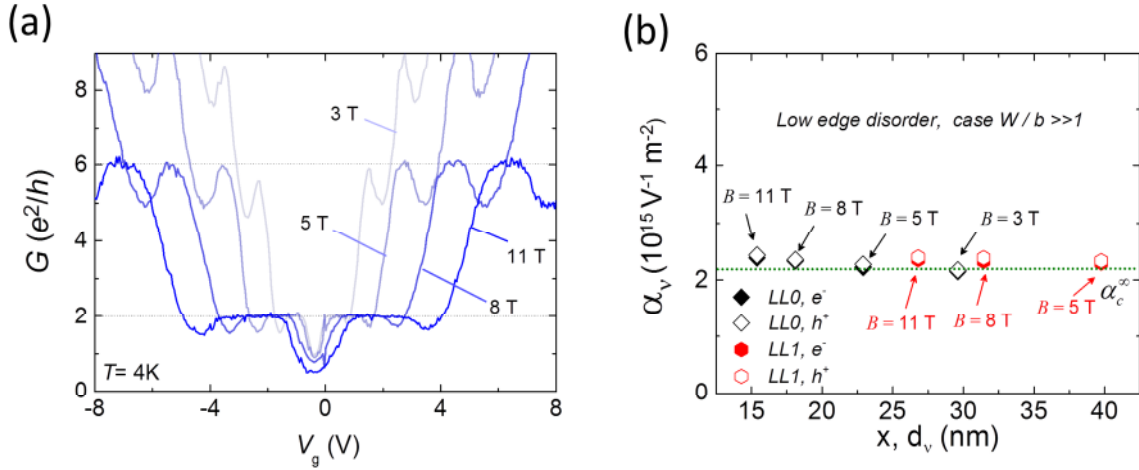


Fig.S2. (a) Two-point (2-pt) magnetoconductance $G(V_g, B)$ of pre-constriction devices (graphene strips of width $W = 1 \mu\text{m}$) at $T = 4 \text{ K}$ and magnetic fields $B = 3, 5, 8$ and 11 T . (b) Experimental effective capacitance α_v across large devices for different Landau Levels (LLs) for electrons (e^-) and holes (h^+) at positions x corresponding to the cyclotron diameter d_v .

Fabrication of nanoconstrictions

The subsequent definition of the nanoconstrictions is done via electron beam lithography (EBL) using polymethyl-methacrylate (PMMA) developed at $-5 \text{ }^\circ\text{C}$ in a 1:3 IPA:H₂O solution. The edge quality in our constrictions is defined with two complementary etching processes: oxygen plasma ashing and reactive ion etching. [S2,S6] Devices with a higher amount of edge disorder (S_{high}) are defined by plasma ashing, which, despite being known to introduce instabilities and localized states in graphene nanodevices, is widely used to shape graphene nanostructures [S6]. In contrast, devices with a much lower amount of edge disorder [S2,S6] (S_{low}) were produced by reactive ion etching (argon 40 sccm, oxygen 5 sccm). We achieve an edge roughness below 1 nm with the latter etching procedure, as demonstrated in Ref. S2. Prior to measuring their electrical properties, we dip our devices for

18h in a pure hexamethyldisilazane (HMDS) solution to reduce the effect of environmental contaminants that may have been adsorbed on the basal plane of graphene or at the edges during the processing steps [S2,S7]. After these 18h, the devices are dipped for 5 s in acetone, 5 s in IPA and then dried with nitrogen.

Both types of nanoconstriction devices S_{high} and S_{low} are limited by boundary scattering [S2]. Apart from a characteristic $G \propto \Delta V_g^{1/2}$ behavior [S2], this is shown by a two-point conductance G as a function of the back-gate V_g not significantly changed at the two measured temperatures $T = 4 \text{ K}$ and $T = 300 \text{ K}$ (Fig. S3).

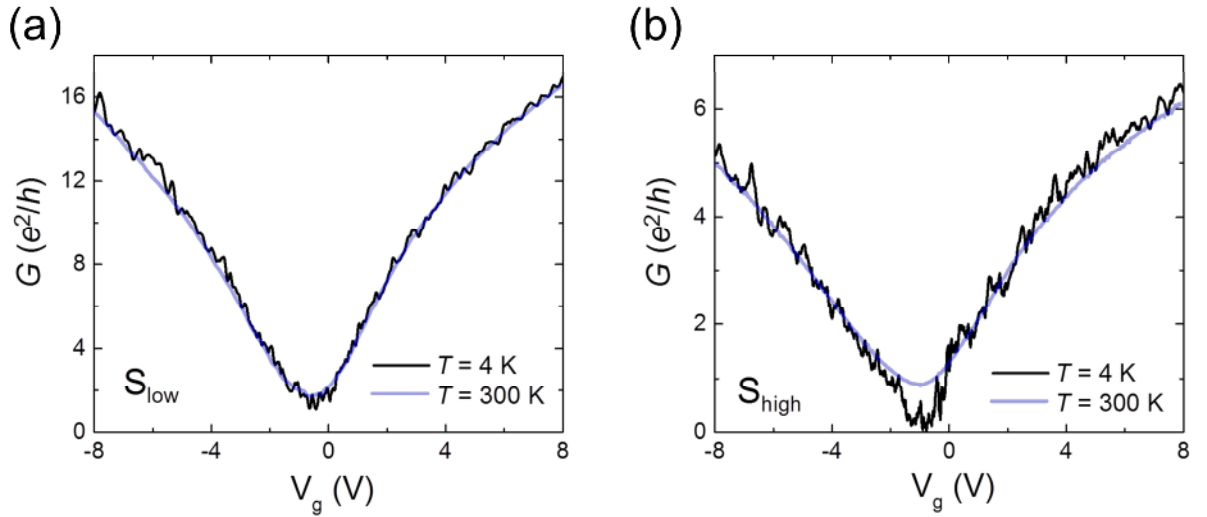


Fig. S3. Conductance measurements in graphene nanoconstrictions at $T=4 \text{ K}$ and $T=300 \text{ K}$ for $B=0 \text{ T}$. **a**, Conductance G as a function of the gate voltage V_g in a graphene nanoconstriction with low edge roughness (S_{low}) at $T = 4 \text{ K}$ (black) and $T = 300 \text{ K}$ (blue). The extracted R_c in this sample is 420Ω . **b**, Conductance G as a function of the gate voltage V_g in graphene nanoconstriction with high edge roughness (S_{high}) at $T=4 \text{ K}$ (black) and $T=300 \text{ K}$ (blue). The extracted R_c in this sample is 520Ω .

2. Validity of the semi-classical method to probe the capacitance profile in the presence of the conductance quantization suppression (CQS) phenomenon.

The CQS phenomenon [S2,S8] is an effect occurring in ballistic and finite-size graphene devices as a consequence of the qualitative modification of the band structure of these gated systems within the quantum Hall regime (Fig. S4a) caused by fringing electrostatic field effects. As such, new, residually overlapping and counter-propagating conducting channels appear at the central part of the device with finite weight over a large portion of the device's width (Fig. S4b, local density of states LDOS). Their presence manifests itself in an increased conductance with respect to the single-particle picture, with suppressed quantization (Fig. 1d, main text) [S2]. Furthermore, as shown in Fig. S5, these features are robust with respect to temperature variations, showing small alterations in the magnetoconductance of the device that could be ascribed [S8] to the density of states (DOS) broadening by the thermal energy.

A detailed theory supporting the validity of the semi-classical method used here to probe the capacitance profile in the presence of fringing electrostatic field effects can be found in Ref.

[S9]. Briefly Ref.[S9] describes how, *i*) the semi-classical approximation $n_\nu(x) = \frac{eB}{h} \nu(x)$ is

valid in these systems subject to fringing electrostatic fields, where the occupation factor $\nu(x)$ varies locally across the device [S10,S11]. Furthermore, *ii*) the position of the additional counter-propagating edge channels in the system and their evolution with respect to the

magnetic field is approximately given by $d_\nu = \sqrt{\frac{\nu h}{e\pi B}}$ [S9].

As such, ν can be directly obtained from the measured conductance $\nu \sim G(e^2 / h)$ [S11] in devices showing the CQS phenomenon in the absence of major backscattering.

In our case, the experimentally observed conductance does (empirically) imply the absence of significant backscattering in nanoconstrictions with low edge roughness (otherwise counterpropagating edge channels would equilibrate [S12,S13]). This is particularly true at $G^{(\max)}$, reaching values $\sim 4e^2/h$ for $LL0$ at $B \leq 12$ T. Thus, it is reasonable to obtain ν at $G^{(\max)}(e^2/h)$ in these systems.

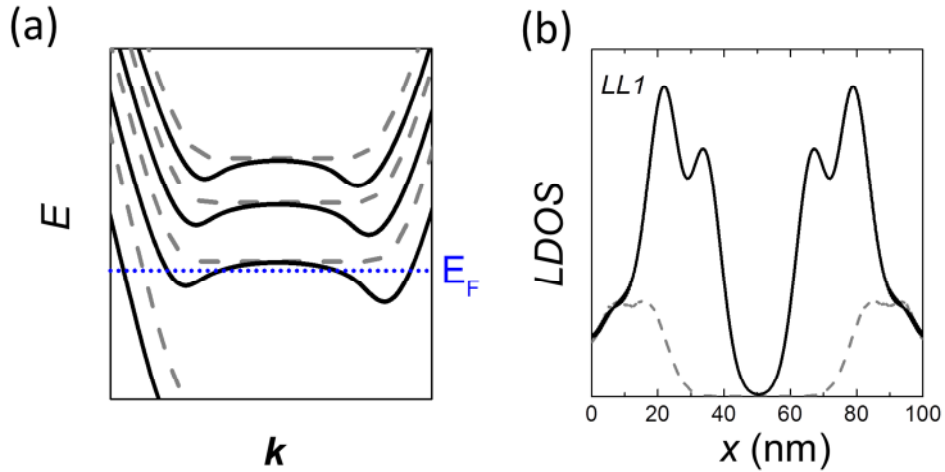


Fig. S4. (a) Band structure near the Fermi level E_F for a ballistic graphene device in the quantum Hall regime accounting (black) and non-accounting (dashed grey) for fringe field effects. (b) Local density of states (LDOS) across a pristine ribbon at a gate voltage that displays a CQS peak for the $LL1$. Fringe field effects (black) introduce states in the ribbon bulk, which are not present for uniform gating (dashed gray).

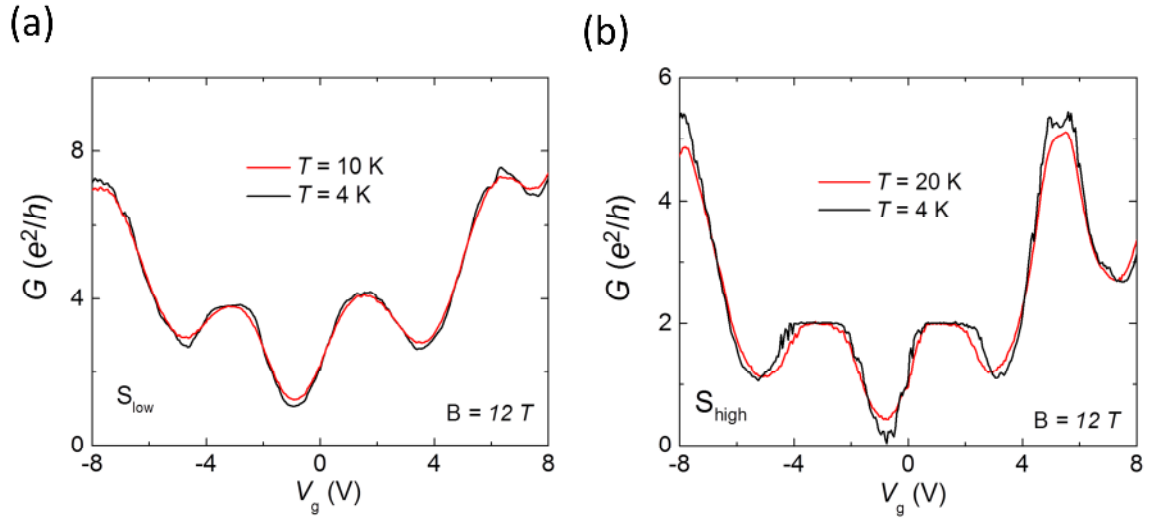


Fig. S5. (a) Measured two-point conductance in our nanoconstriction devices with low edge disorder (S_{low}) at temperatures $T = 4$ K and $T = 10$ K. (b) Measured two-point conductance of our nanoconstriction devices with high edge disorder (S_{high}) at temperatures $T = 4$ K and $T = 20$ K.

3. Electrostatic capacitance calculation $\alpha_c(x)$

Pristine graphene devices exhibit an inhomogeneous, classical capacitance profile $\alpha_c(x)$ diverging towards the device's edges [S4,S5,S14,S15]. $\alpha_c(x)$ can be approximately calculated

considering graphene as a perfect metal [S16] and using $\alpha_c(x) = \frac{n_{w/2}}{V_g} \frac{E_z(x)}{\min(E_z(x))}$ (Fig. S6).

Here, $n_{w/2}$ is carrier density at the centre of the strip (position $x = W/2$). $n_{w/2}$ is obtained by solving the Poisson equation in the device [S12,S16] using a finite-element method solver, at a distance $z = -0.5$ nm (below the graphene plane $z = 0$ nm). For our constrictions ($W = 100$ nm), its value is close to the carrier density for an infinite parallel-plate capacitor, see Fig. S6.

Meanwhile, $\frac{E_z(x)}{\min(E_z(x))}$ is the out of plane, un-screened perpendicular electric field component in the devices [S12], normalized with respect to the minimum value $\min(E_z(x))$

which takes place at the centre of the strip, $W/2 \cdot \frac{E_z(x)}{\min(E_z(x))}$ is obtained at a distance $z = 0.5$ nm above the graphene plane.

Fig. S6 compares $\alpha_c(x)$ for our nanoconstrictions, ribbons of the same width $W = 100$ nm, and the infinite parallel-plate capacitor α_c^∞ . Despite qualitative similarities, for a fixed position x across the devices, the electrostatic capacitance profile in nanoconstrictions is larger than in nanoribbon devices of the same width.

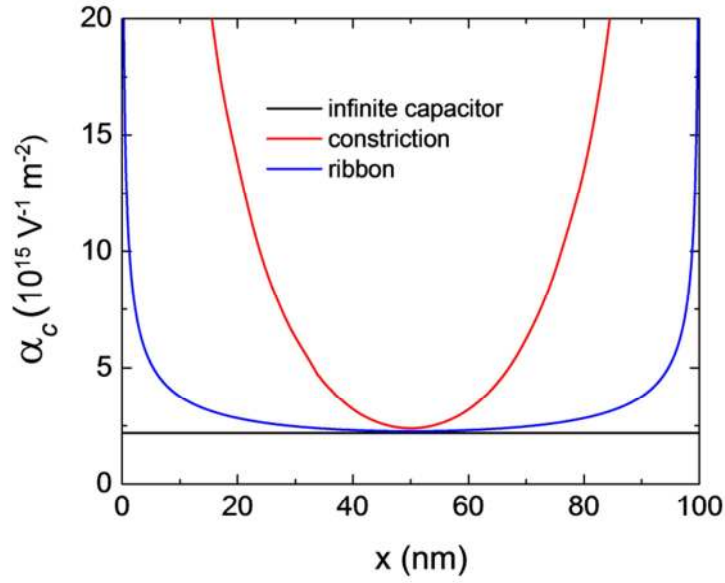


Fig. S6. Electrostatically calculated capacitance $\alpha_c(x)$ across three graphene devices: nanoconstriction with $W = 100$ nm (red), nanoribbon with $W = 100$ nm (blue) and infinite parallel-plate capacitor (black). For a fixed position x , $\alpha_c(x)$ is larger in nanoconstrictions than in nanoribbons with the same width.

4. Quantum capacitance calculation $\alpha_q(x)$ across graphene devices (*LL0* and *LL1*)

We calculate the quantum capacitance contribution $\alpha_q(x)$ across ballistic gated graphene devices from their corresponding LDOS as [S17,S18] $\alpha_q(x) = e|LDOS|$ (Fig. S7). In the present study, LDOS of finite-size and disorder-free graphene devices at $B = 10\text{T}$ are calculated at the two gate voltages corresponding to $G^{(\max)}$ for *LL0* and *LL1*, respectively. Such LDOS calculations are undertaken by using a tight-binding Hamiltonian with a corresponding $U(x) = -\hbar v_F \sqrt{\pi n(x)}$ obtained from the electrostatically capacitance profile $n(x) = \alpha_c(x)V_g$. In other words, we calculate the LDOS of the realistic system, including electrostatic screening effects of the gate potential. Further details about these numerical calculations can be found in Ref. [S2].

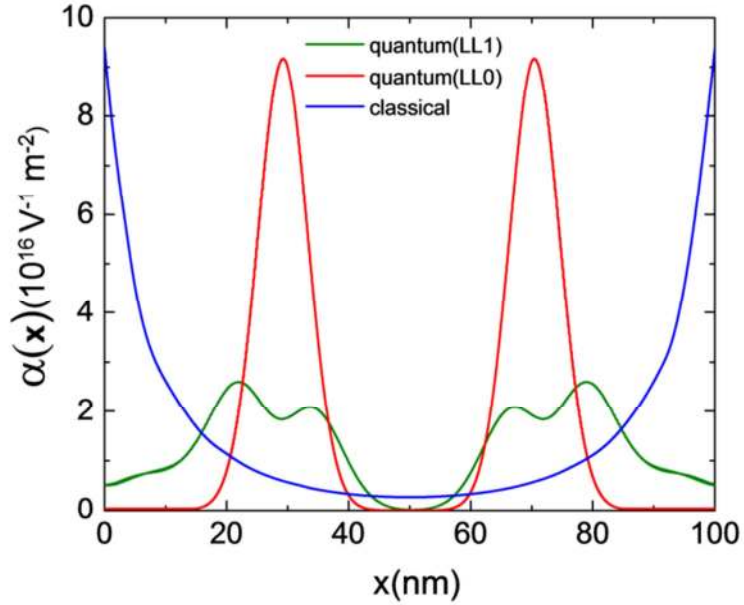


Fig. S7. Quantum capacitance profile for *LL0* (red) and *LL1* (green) across a ballistic graphene device. The classical capacitance profile of our nanoconstrictions (blue) is shown for comparison.

Supplementary References

- S1. M. Lafkioti, B. Krauss, T. Lohmann, U. Zschieschang, H. Klauk, K. von Klitzing and J.H. Smet. Graphene on a hydrophobic substrate: doping reduction and hysteresis suppression under ambient conditions. *NanoLett.*, 2010, 10 (4), 1149 (2010)
- S2. J.M. Caridad, S.R. Power, M.R. Lotz, A.A. Shylau, J.D. Thomsen, L. Gammelgaard, T.J. Booth, A-P. Jauho and P. Bøggild. Conductance quantization suppression in the quantum Hall regime. *Nature. Comm.* (2018).
- S3. L. Gammelgaard, J.M. Caridad, A. Cagliani, D.M.A. Mackenzie, D.H. Petersen, T.J. Booth and P. Bøggild. Graphene transport properties upon exposure to PMMA processing and heat treatments. *2D Mater.* 1, 035005 (2014)
- S4. I.J. Vera-Marun, P.J. Zomer, A. Veligura, M.H.D. Guimarães, L. Visser, N. Tombros, H.J. van Elferen, U. Zeitler and B.J. van Wees. Quantum Hall transport as probe of capacitance profile at graphene edges. *Appl. Phys. Lett.* **102**, 013106 (2013).
- S5. Y-T. Cui, B. Wen, E.Y. Ma, G. Diankov, Z. Han, F. Amet, T. Taniguchi, K. Watanabe, D. Goldhaber-Gordon, C. R. Dean and Z-X. Shen. Unconventional correlation between quantum Hall transport and bulk state filling in gated graphene devices. *Phys. Rev. Lett.*, **117**, 18661 (2016).
- S6. P. Simonet, D. Bischoff, A. Moser, T. Ihn and K. Ensslin. Graphene nanoribbons: relevance of etching process. *J.Appl. Phys.* **117**, 184303-184307 (2015).
- S7. S.F. Chowdhury, S. Sonde, S. Rahimi, L. Tao, S. Banerjee and D. Akinwande. Improvement of graphene field-effect transistors by hexamethyldisilazane surface treatment. *Appl. Phys. Lett.* **105**, 033117-033121 (2014).

- S8. A.A. Shylau, I.V.Zozoulenko, H.Xu and T. Heinzl. Generic suppression of conductance quantization of interacting electrons in graphene nanoribbons in a perpendicular magnetic field. *Phys. Rev. B* **82**, 121410 (2010)
- S9. S.Slizovskiy and V. Fal'ko. Suppressed compressibility of quantum Hall effect edge states in epitaxial graphene on SiC. *Phys. Rev. B* **97**, 075404 (2018).
- S10. A. Siddiki and R.R. Gerhards. Incompressible strips in dissipative Hall bars as origin of quantized Hall plateaus. *Phys. Rev. B* **70**, 195335 (2004)
- S11. D.B. Chklovskii, K.A. Matveev and B.I. Shklovskii. Ballistic conductance of interacting electrons in the quantum Hall regime. *Phys. Rev. B* **47**, 19 (1993)
- S12. P.G. Silvestrov and K.B. Efetov. Charge accumulation at the boundaries of a graphene strip induced by a gate voltage: Electrostatic approach. *Phys. Rev. B*, **77**, 155436 (2008).
- S13. A.A. Shylau and I.V. Zozoulenko. Interacting electrons in graphene nanoribbons in the lowest Landau level. *Phys. Rev. B*, **84**, 075407 (2011)
- S14. J. Fernández-Rossier, J.J. Palacios and L. Brey. Electronic structure of gated graphene and graphene nanoribbons. *Phys. Rev. B* **75**, 205441-205448 (2007).
- S15. Shylau, A.A., Klos, J.W. & Zozoulenko, I.V. Capacitance of graphene nanoribbons. *Phys. Rev. B* **80**, 205402 (2009)
- S16. M.T. Allen, J. Martin and A. Yacoby. Gate-defined quantum confinement in suspended bilayer graphene. *Nature Comm.* **3**, 934-939 (2012).

S17. S. Dröscher, P. Roulleau, F. Molitor, P. Struderus, C. Stampfer, K. Ensslin and T. Ihn. Quantum capacitance and density of states of graphene. *Appl. Phys. Lett.* **96**, 152104 (2010)

S18. R. Reiter, U. Derra, S. Birner, B. Terrés, F. Libisch, J. Burgdörfer and C. Stampfer. Negative quantum capacitance in graphene nanoribbons with lateral gates. *Phys. Rev. B* **84**, 115406 (2014)